Analysis of Nonlinear Fiber Kerr Effects for Arbitrary Modulation Formats

Hami Rabbani, Hamid Hosseinianfar, Hamed Rabbani, Maïté Brandt-Pearce, *Senior Member, IEEE*

***Abstract*—Coherent optical transmission systems can be modeled as a four-dimensional (4D) signal space resulting from the two polarization states, each with two quadratures. Recently, nonlinear analytical models have been proposed capable of capturing the impact of Kerr nonlinearity on 4D constellations. None of these addresses the inter-channel nonlinear interference (NLI) imposed by arbitrary modulation formats in multi-channel wavelength division multiplexed (WDM) systems. In this paper, we introduce a general nonlinear model for multi-channel WDM systems that is valid for arbitrary modulation formats, even asymmetric ones. The proposed model converges to the previous models, including the EGN model, in the special case of polarization multiplexed systems. The model focuses on the cross-phase modulation (XPM) nonlinear term that lies at the heart of the NLI in multi-channel WDM systems operating on standard high dispersion single-mode fiber. We show that strategic mappings of the modulation format's coordinates to the polarization states can reduce the NLI undergone by these formats.**

***Index Terms*—Coherent systems, Channel model, Four-dimensional signal spaces, Inter channel nonlinear interference, Optical Kerr effects, Optical fiber communications.**

I. Introduction

ANALYTICAL nonlinear channel models in optical fiber communications have been developed that provide a powerful tool to estimate the nonlinear interference (NLI) caused by the Kerr nonlinearity. Although the literature provides many such models, most are restricted to polarization multiplexed (PM) modulation formats. This paper presents an analytical nonlinear model that has the power to predict the NLI in systems using an arbitrary modulation format, including those using asymmetric four dimensional (4D) constellations.

The first nonlinear model was introduced in 1993 [1]. Then, an analytical solution to the nonlinear Schrödinger equation employing the Volterra series method was presented both in the time and frequency domains in [2]. Following years of neglect, greater efforts have been made recently to achieve more accurate nonlinear models. The Gaussian noise (GN) model was derived based on the assumption that the transmitted signal in a link follows a Gaussian distribution [3], [4], leading to an overestimate of the NLI. The first 4D GN-like nonlinear model was introduced in [5].

The GN model does not contain any modulation-format-dependent terms. A second-order perturbation technique for the self-phase modulation and cross-phase modulation (XPM) effects was developed in [6]. A modulation-format-dependent time-domain model was proposed for the first time in [7] by resorting to an asymptotic approximation reminiscent of the far-field approximation in paraxial optics. The authors of [8] found that there is a discrepancy between the time domain model in [7] and the GN model [3], and they attributed this deviation to the Gaussianity assumption of the signal in the GN model. To settle this discrepancy, [8] added a modulation-format-dependent correction term to the XPM term. Following the same approach as [8], the authors of [9] added correction terms to the GN model, taking the self-channel interference (SCI), cross-channel interference (XCI), and multi-channel interference (MCI) terms into account, giving rise to an enhanced Gaussian noise (EGN) model.

Other versions of the GN model have emerged to improve its accuracy under different scenarios. Modifications to the GN model to account for the presence of stimulated Raman scattering (SRS) were presented in [10], [11], which are capable of taking into account an arbitrary frequency-dependent signal power profile. These models are valid for Gaussian-modulated signals such as probabilistically-shaped high-order modulation signals. Very recently, [12] proposed an approximate GN model for SCI and cross-phase modulation (XPM) in the presence of SRS. The authors of [13], [14] added a modulation format correction term to the XPM, derived in [12, Eq. (8)], while the SCI was computed under a Gaussian assumption. Modulation-format-dependent models in the presence of SRS were proposed in [15], [16], accounting for all the NLI terms, the SCI, XCI, and MCI. The model in [16] introduced a general link function for heterogeneous fiber spans where the span loss and SRS gain/loss are not fully compensated by the amplifier at the end of each span.

Some nonlinear channel models have targeted space-division multiplexing (SDM) systems. An extended version of the GN model for SDM was proposed in [17], irrespective of modulation format dependence and modal dispersion. A modulation-format-dependent nonlinear model was derived in [18] for SDM fibers taking the variance of XPM into account. A comprehensive nonlinear model for SDM as an extension of [18] was introduced in [19], including all the NLI terms such as the SCI, XCI, and MCI terms.

All of the analytical models described above are valid for PM systems but do not apply to 4D modulated systems. In [20], we derived a nonlinear model which quantifies the impact of Kerr nonlinearity on 4D symmetric constellations, accounting for the SCI and XPM nonlinear terms. We extended the model in [20] to a general nonlinear model [21] that accounts for all the NLI terms, including the SCI, XCI, and MCI terms. Although the model given in [21] has the power

H. Rabbani, H. Hosseinianfar and M. Brandt-Pearce are with the Charles L. Brown Department of Electrical and Computer Engineering, University of Virginia, Charlottesville, VA 22904, USA. E-mails: {dmr3ub, hh9af, mbp}@virginia.edu.

Hamed Rabbani is with the Sina Innovative Communications Systems Corporation, Tehran, Iran. E-mail: hamed.rabbani@sinacomsys.com.

to take all the NLI terms into account, it still lacks the ability to predict the NLI of constellations that lack symmetry. The contribution of the SCI variance for arbitrary modulation formats was derived in [22], but it does not address the NLI terms that disturb multi-channel WDM systems.

In this paper, we derive a nonlinear model for arbitrary 4D constellations capable of capturing the predominant nonlinear term in multi-channel WDM systems, namely the XPM term. The SCI nonlinear term is caused by the interaction between symbols transmitted within the channel of interest (COI) and is much easier to compensate for [8]. The SCI can, for instance, be reduced by a signal processing technique known as backpropagation [23], [24]. For high-speed optical transmission, where multiple WDM channels occupy the C-band spectrum, the predominant nonlinear term in the high dispersion regime comes from the XPM terms [25]. For these reasons, we concentrate on deriving the XPM in this paper, as in [8]. To derive this model, we remove the restricting assumptions made in [20, Sec. III]. The emphasis in this paper is on the high dispersion regime where, for instance, high symbol rates of around 32 Gbaud are used in a single mode fiber (SMF); the proposed model should not be used for predicting the NLI in the low dispersion regime, where the impact of MCI nonlinear terms is significant. The derivation of a general analytical model that accounts for all NLI terms, such as SCI, XCI, and MCI, for an arbitrary modulation format falls outside the scope of this paper and is left to future work.

The significance of our model is its ability to capture the NLI on *any* 4D signal space. Not only does this paper give expressions to evaluate the NLI of asymmetric constellations, which has not been done before for multichannel systems, it also tackles the shortcoming in [20], [21] brought about by the assumptions made therein. There exist 4D symmetric constellations whose NLI cannot be predicted by [20], [21] such as BPSK, SP-QAM4_32 [26], SP-QAM4_512 [26], etc. However, we are able to compute the NLI of such constellation through the model proposed in this paper. Furthermore, we provide final expressions that the reader can directly apply to a wide range of purposes, such as geometric and probabilistic shaping. We benchmark the proposed model against the EGN model, and find that the EGN model may inaccurately predict the NLI by about 1.4 dB for a system with 80 WDM channels. Unique to this work, the model can be used to understand how the alignment of the signal constellation with the light polarization affects the severity of the NLI. In particular, we show that a good mapping of the constellation's coordinates to the polarization states can decrease the NLI up to 0.5 dB in certain scenarios.

The structure of the paper is as follows. In Sec. II, we review the first-order solution to the Manakov equation. Sec. III presents the key result of this work, which is an expression for the XCI power. Sec. IV is devoted to simulation results; a wide range of 4D constellations are compared in terms of the experienced XCI in this section. Sec. V provides the conclusion. Finally, the appendix provides a detailed derivation of the NLI model.

Notation: We use $(\cdot)_{\mathrm{x}}$ and $(\cdot)_{\mathrm{y}}$ in this paper to refer to variables related to polarizations x and y, respectively. Two dimensional complex functions are designated by boldface symbols. The conjugate transpose is denoted by $(\cdot)^\dagger$, whereas expectations are indicated by $\mathbb{E}\{\cdot\}$.

II. Preliminaries

To describe the signal transmission, we start from the Manakov equation[1]

$$\frac{\partial}{\partial z}\boldsymbol{u}(t,z) = -\frac{i\beta_2}{2}\frac{\partial^2}{\partial t^2}\boldsymbol{u}(t,z) + i\frac{8}{9}\gamma f(z)\boldsymbol{u}^\dagger(t,z)\boldsymbol{u}(t,z)\boldsymbol{u}(t,z), \quad (1)$$

in which $\boldsymbol{u}(t,z)$ is associated with the electrical field $\boldsymbol{E}(t,z)$, given in [20, Eq. (1)], by rescaling it to cancel out the attenuation contribution. The function $f(z)$ is responsible for the link's loss/gain profile, which is equal to 1 in the case of perfectly distributed amplification, and equal to $\exp\{-\alpha \mathrm{mod}(z,L)\}$ in the case of lumped amplification where α is the loss coefficient, L is the span length, and $\mathrm{mod}(z,L)$ indicates the distance between the point z and the nearest preceding amplifier. In (1), β_2 is the group velocity dispersion and γ is the fiber nonlinearity coefficient.

Throughout this work, our main focus is on interference due to the XPM effect. This effect involves only two-channel interactions, and as a result, the NLI contributions of multiple WDM channels add up independently. We thus carry out our initial analysis with only two channels, of which one is the channel of interest (COI), whose central frequency is arbitrarily set to zero, and the other is an interfering channel with central frequency Ω. The linear solution to (1) for two channels is then expressed as

$$\boldsymbol{u}(z,t) = \sum_k \boldsymbol{a}_k g_a(t-kT_a,z) + \mathrm{e}^{-i\Omega t + \frac{i\beta_2\Omega^2}{2}z}\sum_k \boldsymbol{b}_k g_b(t-kT_b-\beta_2\Omega z, z), \quad (2)$$

where $\boldsymbol{a}_k$ and $\boldsymbol{b}_k$ represent the k-th symbol transmitted in the COI and the interfering channel, respectively. The dispersed pulse waveform at point z along the fiber is $g_{a,b}(t,z) = \exp(-iz\beta_2/2\partial_t^2)g_{a,b}(t,0)$, where $g_{a,b}(t,0)$ is the injected waveform and ∂_t^2 is the time derivative operator. The symbol durations of the COI and interfering channel are denoted by T_a and T_b, respectively. The COI is matched filtered with a filter whose impulse response is proportional to $g_a^*(L,t)$. Without loss of generality, we aim to detect the zeroth symbol $\boldsymbol{a}_0$.

The extracted symbol at the receiver may be expressed as $\boldsymbol{a}_0 + \Delta\boldsymbol{a}_0$, where $\Delta\boldsymbol{a}_0$ accounts for the NLI. By resorting to a perturbation approach, we can write the first-order solution of the Manakov equation as

$$\Delta\boldsymbol{a}_0(\Omega) = i\frac{8}{9}\gamma\sum_{h,k,l} S_{h,k,l}\boldsymbol{a}_k^\dagger\boldsymbol{a}_h\boldsymbol{a}_l + i\frac{8}{9}\gamma\sum_{h,k,l} X_{h,k,l}\left(\boldsymbol{b}_k^\dagger\boldsymbol{b}_h\mathbb{I} + \boldsymbol{b}_h\boldsymbol{b}_k^\dagger\right)\boldsymbol{a}_l, \quad (3)$$

[1]It was first shown in [27] that the coupled nonlinear Schrödinger equation that describes wave evolution over long length along a communication fiber can be reduced to the Manakov equation.

where $\mathbb{I}$ is the 2×2 identity matrix, and $S_{h,k,l}$ and $X_{h,k,l}$ are expressed as

$$S_{h,k,l}=\int_0^L \mathrm{d}z\int_{-\infty}^{\infty}\mathrm{d}t f(z)g_a^*(t,z)g_a(t-lT_a,z)\cdot g_a^*(t-kT_a,z)g_a(t-hT_a,z), \tag{4}$$

and

$$X_{h,k,l}=\int_0^L \mathrm{d}z\int_{-\infty}^{\infty}\mathrm{d}t f(z)g_a^*(t,z)g_a(t-lT_a,z)\cdot g_b^*(t-kT_b-\beta_2\Omega z,z)g_b(t-hT_b-\beta_2\Omega z,z), \tag{5}$$

respectively. The SCI and XPM terms are obtained via the first and second summations on the right-hand side of (3), respectively. We concentrate exclusively on the XPM term because the impact of the SCI was already described in [22]. Using the fact that $g(t,z)=\int \mathrm{d}w\tilde{g}(w)\exp(-iwt+iw^2\beta_2 z/2)/(2\pi)$, where $\tilde{g}(w)$ is the Fourier transform of $g(t,0)$, (5) can be written in the frequency domain as

$$X_{h,k,l}=\int \frac{\mathrm{d}^3 w}{(2\pi)^3}\rho(w_1,w_2,w_3)\mathrm{e}^{i(w_1h-w_2k+w_3l)T}, \tag{6}$$

where $\int \mathrm{d}^3 w$ signifies $\int\int\int \mathrm{d}w_1\mathrm{d}w_2\mathrm{d}w_3$, and

$$\rho(w_1,w_2,w_3)=\tilde{g}_a^*(w_1-w_2+w_3)\tilde{g}_b(w_1)\tilde{g}_b^*(w_2)\tilde{g}_a(w_3)\cdot\int_0^L \mathrm{d}z f(z)\mathrm{e}^{i\beta_2(w_2-w_3+\Omega)(w_2-w_1)z}. \tag{7}$$

The x-polarized and y-polarized components of the second term of (3) can be assembled into a vector denoted as $\Delta\boldsymbol{a}_{\text{XPM},0}$ with components

$$\Delta a_{\text{XPM},0,\mathrm{x}}(\Omega)=i\frac{8}{9}\gamma\sum_{h,k,l}X_{h,k,l}\Big(2b_{h,\mathrm{x}}b_{k,\mathrm{x}}^*a_{l,\mathrm{x}}+b_{h,\mathrm{y}}b_{k,\mathrm{y}}^*a_{l,\mathrm{x}}+b_{h,\mathrm{x}}b_{k,\mathrm{y}}^*a_{l,\mathrm{y}}\Big), \tag{8}$$

and

$$\Delta a_{\text{XPM},0,\mathrm{y}}(\Omega)=i\frac{8}{9}\gamma\sum_{h,k,l}X_{h,k,l}\Big(2b_{h,\mathrm{y}}b_{k,\mathrm{y}}^*a_{l,\mathrm{y}}+b_{h,\mathrm{x}}b_{k,\mathrm{x}}^*a_{l,\mathrm{y}}+b_{h,\mathrm{y}}b_{k,\mathrm{x}}^*a_{l,\mathrm{x}}\Big). \tag{9}$$

The reader is referred to [20, Eq. 2], [28, Appendix], [8], and [7, Sec. II] to find the origin of (1)-(9).

III. Key result at a glance: The NLI Power

In this section, we give the final result of the paper, making the resulting expressions easily accessible to the reader. Detailed derivations are relegated to the Appendix.

To obtain the key result, we remove some of the simplifying assumptions made in [20, Sec. III] except the following. We first assume that the data symbols in the x- and y-polarization are correlated with each other. Channels across the spectrum can have different 4D modulation formats. The modulations are assumed to be zero mean, i.e., $\mathbb{E}\{a_{\mathrm{x}}\}=\mathbb{E}\{a_{\mathrm{y}}\}=0$. In our expressions, channels within the spectrum have the same launch power, an assumption which can be easily removed to generalize the results. The key result is obtained for Nyquist rectangular spectral shape channels (sinc pulses) [3], [8], [9], yet we note that our model has the ability to compute the nonlinear disturbance resulting from near rectangular signal spectral shapes, such as a root raised cosine with a small roll-off factor [3]. Note that we no longer assume that the modulation's constellation is symmetric with respect to the two polarizations.

Given (3), the NLI covariance of the zeroth symbol of the COI is given by

$$\mathrm{Cov}(\Delta\boldsymbol{a}_{\text{XPM},0})=\mathbb{E}\Big\{(\Delta\boldsymbol{a}_{\text{XPM},0}-\mathbb{E}\{\Delta\boldsymbol{a}_{\text{XPM},0}\})\cdot(\Delta\boldsymbol{a}_{\text{XPM},0}-\mathbb{E}\{\Delta\boldsymbol{a}_{\text{XPM},0}\})^{\dagger}\Big\}, \tag{10}$$

in which we suppressed the indication of the Ω-dependence in $\Delta a_{\text{XPM},0}$ for notational convenience. Because $\mathbb{E}\{\Delta a_{\text{XPM},0}\}$ is equal to zero, (10) can be written as

$$\mathrm{Cov}(\Delta\boldsymbol{a}_{\text{XPM},0})=\begin{bmatrix}\mathbb{E}\{\Delta a_{\text{XPM},0,\mathrm{x}}\Delta a_{\text{XPM},0,\mathrm{x}}^*\} & \mathbb{E}\{\Delta a_{\text{XPM},0,\mathrm{x}}\Delta a_{\text{XPM},0,\mathrm{y}}^*\}\\ \mathbb{E}\{\Delta a_{\text{XPM},0,\mathrm{y}}\Delta a_{\text{XPM},0,\mathrm{x}}^*\} & \mathbb{E}\{\Delta a_{\text{XPM},0,\mathrm{y}}\Delta a_{\text{XPM},0,\mathrm{y}}^*\}\end{bmatrix}, \tag{11}$$

Although the non-diagonal terms of the covariance matrix in (11) are non-zero, the power of the NLI on the COI caused by the second term of (3) depends only on the diagonal terms and can be written as

$$P_{\text{XPM}}(\Omega)=\mathrm{trace}\left[\mathrm{Cov}\left\{\Delta\boldsymbol{a}_{\text{XPM},0}\right\}\right] \tag{12}$$

$$=\sigma^2_{\text{XPM},\mathrm{x}}(\Omega)+\sigma^2_{\text{XPM},\mathrm{y}}(\Omega), \tag{13}$$

where $\sigma^2_{\text{XPM},\mathrm{x}}$ and $\sigma^2_{\text{XPM},\mathrm{y}}$ are the XPM variances on polarizations x and y, respectively. The term $\sigma^2_{\text{XPM},\mathrm{x}}$, given in (13), results in the final expression

$$\sigma^2_{\text{XPM},\mathrm{x}}(\Omega)=\mathbb{E}\{\Delta a_{\text{XPM},0,\mathrm{x}}\Delta a_{\text{XPM},0,\mathrm{x}}^*\}=\frac{64}{81}\gamma^2P_{\mathrm{x}}^3\Big(\Phi_1(\Omega)\chi_1(\Omega)+\Phi_2(\Omega)Z(\Omega)+\Phi_3(\Omega)\chi_2(\Omega)\Big), \tag{14}$$

where P_{x} is the launch power in polarization x so that the total optical transmit power becomes

$$P=P_{\mathrm{x}}+P_{\mathrm{y}}. \tag{15}$$

The terms $\chi_1(\Omega)$, $Z(\Omega)$, and $\chi_2(\Omega)$ in Table I depend on the spectral properties of the signal. The terms Φ_1, Φ_2 and Φ_3 in Table II, on the other hand, depend on the modulation format. The term $\sigma^2_{\text{XPM},\mathrm{y}}$, given in (13), can be obtained from (14) by swapping x and y in these equations and the terms given in Table II. A detailed derivation of (14) is given in the Appendix. In the special case of independent polarizations where the same format is used in both polarizations, Table II reduces to $\Phi_1=5\mathbb{E}\{|b_{\mathrm{x}}|^4\}/\mathbb{E}^2\{|b_{\mathrm{x}}|^2\}-10$, $\Phi_2=6$, and $\Phi_3=0$. These values used in combination with the integral expressions in Table I can be shown to coincide with the EGN model.

As mentioned above, the NLI contributions stemming from multiple channels in a multi-channel WDM system add up independently. The total NLI power on the n-th channel in the spectrum resulting from the XPM contributions of N WDM

Table I
INTEGRAL EXPRESSIONS FOR THE TERMS USED IN (14).

Term	Integral Expression
χ_1	$\frac{1}{T^2}\int \frac{\mathrm{d}^3 w}{(2\pi)^3}\frac{\mathrm{d}w_2'}{2\pi}\rho(w_1,w_2,w_3)\rho^*(w_1-w_2+w_2',w_2',w_3)$
Z	$\frac{1}{T^3}\int \frac{\mathrm{d}^3 w}{(2\pi)^3}\lvert\rho(w_1,w_2,w_3)\rvert^2$
χ_2	$\frac{1}{T^3}\int \frac{\mathrm{d}^3 w}{(2\pi)^3}\rho(w_1,w_2,w_3)\rho^*(-w_2,-w_1,w_3)$

channels can be expressed as

$$P_{\mathrm{NLI},n} = \sum_{i=1, i\neq n}^{N} P_{\mathrm{XPM}}(\Omega_{i,n}), \quad \Omega_{i,n} = |\nu_i - \nu_n|. \tag{16}$$

where the function $P_{\mathrm{XPM}}(\cdot)$ is provided in (12). In (16), ν_i is the central frequency of channel i.

IV. NUMERICAL RESULTS

In this section, we first numerically validate our model using the split-step Fourier method (SSFM), described in detail in [20, Sec. III], for an optical fiber communication system accommodating 80 WDM channels, using the parameters listed in Table III. We then compare a wide range of 4D modulation formats regarding the NLI experienced in a fully-loaded C band transmission system. Lastly, we investigate how different mappings of the constellation's coordinates to the polarization states may affect the NLI experienced.

A. SSFM validation

In this section, we compare our model with the classical EGN model (the XPM term given in [9, Eqs. (14)–(17)]) as a benchmark in a fully-loaded C-band transmission. Fig. 1 shows the SNR of the COI, channel $n = 40$,

$$\mathrm{SNR}_{40} = \frac{P}{\sigma^2_{\mathrm{ASE}} + P_{\mathrm{NLI},40}}, \tag{17}$$

where σ^2_{ASE} is the amplified spontaneous emission noise generated by the EDFA amplifiers along the link, as a function of launch power for 16-, 256-, and 4096-point constellations. In order to validate (17), SSFM numerical simulations were conducted. Specifically, (17) can be estimated by the simulated SNR of the 40th channel; for a constellation with M symbols, the SNR was estimated through

$$\mathrm{SNR}^{\mathrm{est}}_{40} = \frac{\sum_{i=1}^{M}|\bar{y}_i|^2}{\sum_{i=1}^{M}\mathbb{E}\{|Y-\bar{y}_i|^2|X=x_i\}}, \tag{18}$$

where X and Y are the random variables representing the transmitted and received symbols, respectively, x_i is the i-th constellation point, and $\bar{y}_i = \mathbb{E}\{Y|X=x_i\}$. A total of 2^{15} symbols were simulated per data point, of which the first and last 1500 symbols were removed from the transmitted and received sequences. All channels used the same launch power. In Fig. 1, we mark the SSFM results as filled circles. The modulation formats considered in our simulations are PM-QPSK, subset optimized PM-QPSK (SO-PM-QPSK) [29], [30], c4_16 [31], [32], PM-16QAM, voronoi4_256 [33], [34], a4_256 [35], w4_256 [36], PM-64QAM, and a4_4096 [32].

Our proposed model, labeled as the 4D model, closely follows the results obtained via SSFM for all types of 4D formats shown in Fig. 1. By contrast, the gap between the conventional EGN model results (marked as dashed curves in Fig. 1) and the SSFM results shows the obvious shortcoming of the EGN model in predicting the NLI of 4D formats. From these results, we expect our model to be precise enough to predict the NLI in systems using any modulation type and operating in the high dispersion regime in which the chief NLI terms are the SCI and XPM. We found in our simulations that the discrepancy between the results of the model proposed and the SSFM results becomes greater as the channel spacing decreases. For systems operating at low symbol rates, this gap also increases. The main reason for this deviation is the impact of MCI nonlinear terms ignored in this paper. Note that for PM modulation formats that do not violate the assumptions made in [20], [21], our model yields the same results as the EGN model.

B. Analysis of the NLI undergone by channels across the spectrum

In this section we further analyze the experienced NLI of all channels across the spectrum using the parameters listed in Table III. The 4D modulation formats tested, selected from [30], are compared using the NLI noise experienced by channel n normalized by P^{-3},

$$\eta_n = \frac{P_{\mathrm{NLI},n}}{P^3}, \tag{19}$$

where $P_{\mathrm{NLI},n}$, defined in (16), is the NLI power at the COI. We assume that the whole spectrum can accommodate 80 WDM channels in a system with 50 GHz channel spacing and a symbol rate of 32 Gbaud. We use Eqs. (13)–(14), and Tables I and II to evaluate the NLI of the 4D constellations.

The figures in this section show η_n as a function of the spectral location of the COI, identified by the channel number n. In Fig. 2, we compare 16-point, 256-point, and 4096-point constellations in terms of the NLI experienced. We first note that the symmetry of the results in Fig. 2 indicates that the channels located at either edge of the spectrum experience lower NLI than the ones in the middle. The EGN model results are marked as dashed lines. As can be seen in Fig. 2 (a), the EGN model results are inaccurate for estimating the NLI for the 4D 16-point constellations considered. The EGN model overestimates the NLI encountered by c4_16 format. In contrast, the EGN model underestimates the NLI of SO-PM-QPSK. The difference between the NLI obtained from the EGN model and our proposed model is more pronounced for the c4_16 format, with a gap of about 1.4 dB as shown in Fig. 2 (a).

Fig. 2 (a) also shows that all three 4D formats experience higher NLI than PM-QPSK, meaning that PM-QPSK outperforms 4D peers. SO-PM-QPSK is the most nonlinearity-prone constellation; the difference between the experienced NLI for SO-PM-QPSK and PM-QPSK is about 1.70 dB. The c4_16 format proposed in [31], although exquisitely evolved

Table II
EXPRESSIONS FOR THE MODULATION-DEPENDENT TERMS USED IN (14).

Term	Expression
Φ_1	$\frac{1}{\mathbb{E}\{\lvert a_x\rvert^2\}\mathbb{E}^2\{\lvert b_x\rvert^2\}}\Big(4\mathbb{E}\{\lvert b_x\rvert^4\}\mathbb{E}\{\lvert a_x\rvert^2\} - 8\mathbb{E}\{\lvert a_x\rvert^2\}\mathbb{E}^2\{\lvert b_x\rvert^2\} - 4\mathbb{E}\{b_x^{*2}\}\mathbb{E}\{b_x^2\}\mathbb{E}\{\lvert a_x\rvert^2\}$ $+2\mathbb{E}\{a_x a_y^*\}\mathbb{E}\{\lvert b_x\rvert^2 b_x^* b_y\} - 4\mathbb{E}\{a_x a_y^*\}\mathbb{E}\{b_x^* b_y\}\mathbb{E}\{\lvert b_x\rvert^2\}$ $-2\mathbb{E}\{a_x a_y^*\}\mathbb{E}\{b_x^{*2}\}\mathbb{E}\{b_x b_y\} + 4\mathbb{E}\{\lvert b_x\rvert^2\lvert b_y\rvert^2\}\mathbb{E}\{\lvert a_x\rvert^2\} - 4\mathbb{E}\{\lvert b_y\rvert^2\}\mathbb{E}\{\lvert a_x\rvert^2\}\mathbb{E}\{\lvert b_x\rvert^2\}$ $-4\mathbb{E}\{b_x b_y^*\}\mathbb{E}\{b_y b_x^*\}\mathbb{E}\{\lvert a_x\rvert^2\} - 4\mathbb{E}\{b_x b_y\}\mathbb{E}\{b_x^* b_y^*\}\mathbb{E}\{\lvert a_x\rvert^2\} + \mathbb{E}\{\lvert b_y\rvert^4\}\mathbb{E}\{\lvert a_x\rvert^2\}$ $-2\mathbb{E}^2\{\lvert b_y\rvert^2\}\mathbb{E}\{\lvert a_x\rvert^2\} - \mathbb{E}\{b_y^2\}\mathbb{E}\{b_y^{*2}\}\mathbb{E}\{\lvert a_x\rvert^2\} + \mathbb{E}\{a_x a_y^*\}\mathbb{E}\{\lvert b_y\rvert^2 b_x^* b_y\}$ $-2\mathbb{E}\{a_x a_y^*\}\mathbb{E}\{\lvert b_y\rvert^2\}\mathbb{E}\{b_x^* b_y\} - \mathbb{E}\{a_x a_y^*\}\mathbb{E}\{b_y^2\}\mathbb{E}\{b_x^* b_y^*\} + 2\mathbb{E}\{a_y a_x^*\}\mathbb{E}\{\lvert b_x\rvert^2 b_y^* b_x\}$ $-4\mathbb{E}\{a_y a_x^*\}\mathbb{E}\{b_y^* b_x\}\mathbb{E}\{\lvert b_x\rvert^2\} - 2\mathbb{E}\{a_y a_x^*\}\mathbb{E}\{b_x^2\}\mathbb{E}\{b_x^* b_y^*\} + \mathbb{E}\{a_y a_x^*\}\mathbb{E}\{\lvert b_y\rvert^2 b_x b_y^*\}$ $-2\mathbb{E}\{a_y a_x^*\}\mathbb{E}\{\lvert b_y\rvert^2\}\mathbb{E}\{b_x b_y^*\} - \mathbb{E}\{a_y a_x^*\}\mathbb{E}\{b_y^{*2}\}\mathbb{E}\{b_x b_y\} + \mathbb{E}\{\lvert a_y\rvert^2\}\mathbb{E}\{\lvert b_x\rvert^2\lvert b_y\rvert^2\}$ $-\mathbb{E}\{\lvert a_y\rvert^2\}\mathbb{E}\{b_x b_y^*\}\mathbb{E}\{b_x^* b_y\} - \mathbb{E}\{\lvert a_y\rvert^2\}\mathbb{E}\{\lvert b_y\rvert^2\}\mathbb{E}\{\lvert b_x\rvert^2\} - \mathbb{E}\{\lvert a_y\rvert^2\}\mathbb{E}\{b_x b_y\}\mathbb{E}\{b_x^* b_y^*\}\Big)$
Φ_2	$\frac{1}{\mathbb{E}\{\lvert a_x\rvert^2\}\mathbb{E}^2\{\lvert b_x\rvert^2\}}\Big(4\mathbb{E}\{\lvert a_x\rvert^2\}\mathbb{E}^2\{\lvert b_x\rvert^2\} + 2\mathbb{E}\{b_x^* b_y\}\mathbb{E}\{a_x a_y^*\}\mathbb{E}\{\lvert b_x\rvert^2\} + 4\mathbb{E}\{b_x^* b_y\}\mathbb{E}\{b_x b_y^*\}\mathbb{E}\{\lvert a_x\rvert^2\}$ $+\mathbb{E}^2\{\lvert b_y\rvert^2\}\mathbb{E}\{\lvert a_x\rvert^2\} + \mathbb{E}\{\lvert b_y\rvert^2\}\mathbb{E}\{b_x^* b_y\}\mathbb{E}\{a_x a_y^*\} + 2\mathbb{E}\{b_x b_y^*\}\mathbb{E}\{a_y a_x^*\}\mathbb{E}\{\lvert b_x\rvert^2\}$ $+\mathbb{E}\{\lvert b_y\rvert^2\}\mathbb{E}\{b_x b_y^*\}\mathbb{E}\{a_y a_x^*\} + \mathbb{E}\{\lvert b_y\rvert^2\}\mathbb{E}\{\lvert a_y\rvert^2\}\mathbb{E}\{\lvert b_x\rvert^2\}\Big)$
Φ_3	$\frac{1}{\mathbb{E}\{\lvert a_x\rvert^2\}\mathbb{E}^2\{\lvert b_x\rvert^2\}}\Big(4\mathbb{E}\{b_x^2\}\mathbb{E}\{b_x^{*2}\}\mathbb{E}\{\lvert a_x\rvert^2\} + 2\mathbb{E}\{b_x^{*2}\}\mathbb{E}\{b_x b_y\}\mathbb{E}\{a_x a_y^*\} + 4\mathbb{E}\{b_x^* b_y^*\}\mathbb{E}\{b_x b_y\}\mathbb{E}\{\lvert a_x\rvert^2\}$ $+\mathbb{E}\{b_y^2\}\mathbb{E}\{b_y^{*2}\}\mathbb{E}\{\lvert a_x\rvert^2\} + \mathbb{E}\{b_y^2\}\mathbb{E}\{b_x^* b_y^*\}\mathbb{E}\{a_x a_y^*\} + 2\mathbb{E}\{b_x^2\}\mathbb{E}\{b_x^* b_y^*\}\mathbb{E}\{a_y a_x^*\}$ $+\mathbb{E}\{b_x b_y\}\mathbb{E}\{b_y^{*2}\}\mathbb{E}\{a_y a_x^*\} + \mathbb{E}\{b_x b_y\}\mathbb{E}\{b_x^* b_y^*\}\mathbb{E}\{\lvert a_y\rvert^2\}\Big)$

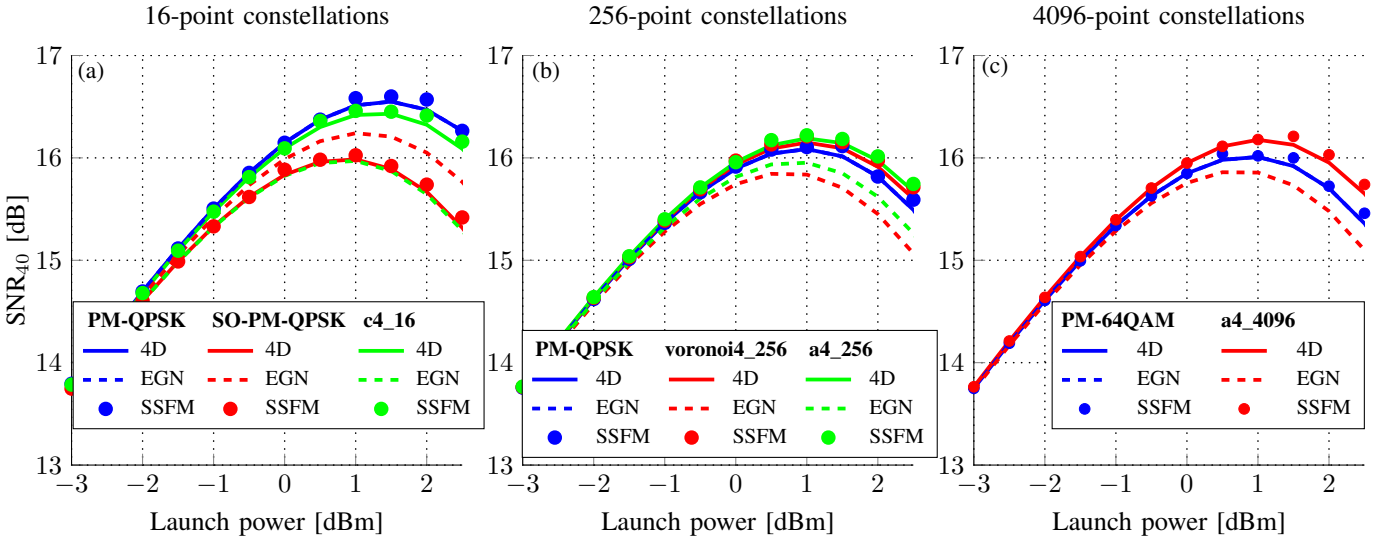

Figure 1. SNR of the COI, the channel located in the middle of spectrum $n = 40$, as a function of launch power after 10 spans of SMF. The full C-band spectrum accommodates N = 80 WDM channels with symbol rate 32 Gbaud and spacing 50 GHz. The SSFM simulation results are marked as filled circles, while the results obtained from the proposed model, labeled as '4D', are marked as solid lines. The benchmark EGN model is denoted using dashed lines.

Table III
SYSTEM PARAMETERS FOR NUMERICAL SIMULATIONS

Parameters	**Values**
Loss (α) [dB/km]	0.22
Dispersion (D) [ps/nm/km]	16.5
Nonlinear coefficient (γ) [1/W/km]	1.3
Span length (L) [km]	100
Symbol rate (R) [Gbaud]	32
Roll-off factor [%]	0.01
Channel spacing (R) [GHz]	50
Number of channels	80
Optical center wavelength (nm)	1550
Optical bandwidth (B_{tot}) [THz]	4
Noise figure (dB)	5

to increase the power efficiency, is more vulnerable to the destructive effect of Kerr nonlinearity than its 2D counterpart (PM-QPSK). Although the mean of the c4_16 constellation is not exactly zero, is it close enough so that the 4D model is able to accurately approximate the NLI experienced. The experienced NLI disparities between different 4D modulation formats is attributed to Φ_1, Φ_2, and Φ_3, defined in Table II and used in (14). Table IV quantifies the influence of Φ_1, Φ_2, and Φ_3, and as a result, χ_1, χ_2, and Z, given in (14), on the NLI. Among the terms shown in this table, Φ_3 has the lowest value, implying that χ_2 in (14) has the least impact on the NLI. The terms Φ_1 and Φ_2, on the other hand, are the dominant factors affecting the NLI.

Fig. 2 (b) shows the NLI undergone by PM-16QAM, voroni4-256, a4_256, and w4_256 formats. In this case, the EGN model overestimates the NLI of the 4D modulations,

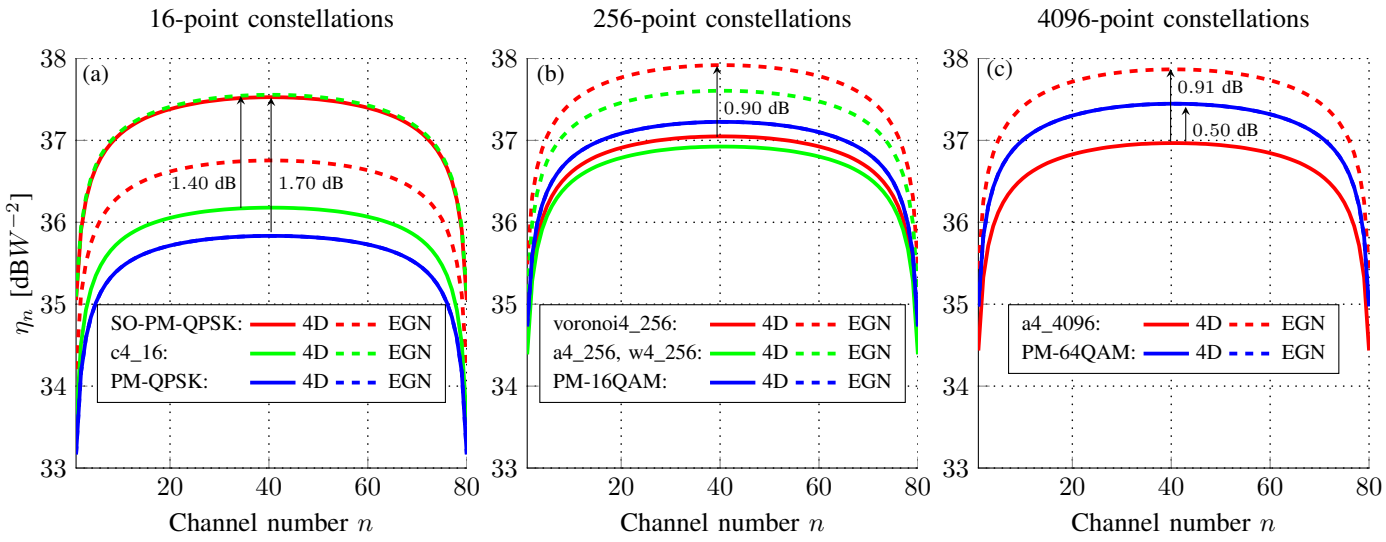

Figure 2. Normalized nonlinear interference η_n defined in (19) as a function of the channel number n after 10 spans of SMF fiber accommodating $N = 80$ 50 GHz WDM channels with symbol rate 32 Gbaud. We call the proposed model '4D', and benchmark this model against the conventional EGN model.

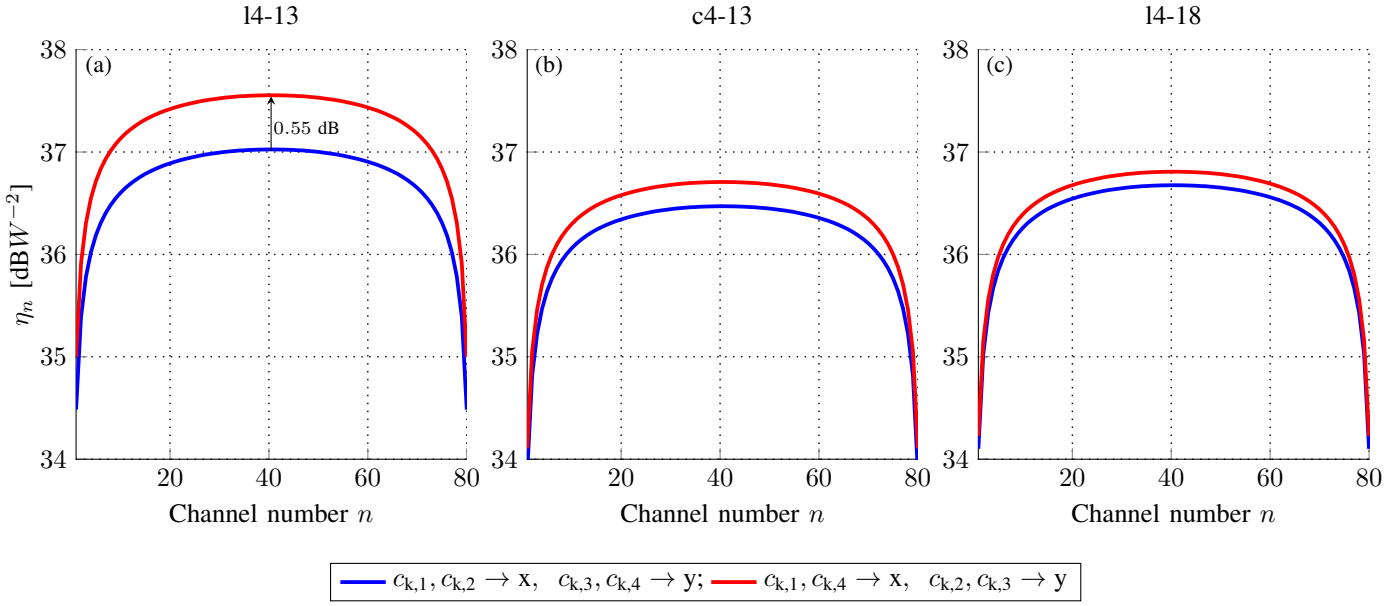

Figure 3. Normalized nonlinear interference η_n defined in (19) as a function of channel number n after 10 spans of SFM fiber. Different mappings of coordinates of l4-13, c4-13 and l4-18 to the fiber polarization states are shown.

voronoi4_256 and a4_256 (rotated w4_256), by around 0.90 dB and 0.80 dB, respectively. Unlike the 16-point constellations, the 256-point 2D modulation, PM-16QAM, is at a disadvantage in comparison with its 4D peers. The difference in NLI between the PM-16QAM and the a4_256/w4-256 formats is about 0.3 dB. This deviation may be rooted in the value of Φ_1, shown in Table IV, which is smaller for a4_256/w4-256 ($\Phi_1 = -3.8$) than for PM-16QAM ($\Phi_1 = -3.4$).

Recall that a4_256 is equivalent to w4_256 by rotation [30]. As can be seen in Fig. 2 (b), there is no change in the NLI between a4-256 and w4-256, meaning that rotations of the constellation do not affect the NLI.

Fig. 2 (c) finally compares PM-64QAM and a4_4096 [30] regarding the experienced NLI. An inaccuracy of around 0.91 dB is seen in the NLI predicted by the EGN model, leading to an overestimate of the NLI. Looking at this figure, we can see that a4_4096 is more resistant to NLI than PM-64QAM and experiences roughly 0.50 dB lower NLI than PM-64QAM.

C. Influence of a constellation's coordinates on the NLI

In this section, we investigate the effects that a constellation's coordinates may have on the NLI. The symbol alphabet, or constellation, of a 4D modulation format with M symbols is given by the set of vectors

$$\mathcal{C} = \{\boldsymbol{c}_1, \boldsymbol{c}_2, \cdots, \boldsymbol{c}_M\}, \tag{20}$$

where $\boldsymbol{c}_k = (c_{k,1}, c_{k,2}, c_{k,3}, c_{k,4})$, of which two are mapped onto the x polarization and the other two onto the y. Different

Table IV
VALUE OF Φ_1, Φ_2, AND Φ_3, GIVEN IN TABLE II, FOR THE CONSTELLATIONS STUDIED IN FIGS. 1 AND 2.

Constellations	Φ_1	Φ_2	Φ_3
PM-QPSK	-5	6	0
c4_16	-5	6.26	0.004
SO-PM-QPSK	-3	6	0
PM-16QAM	-3.40	6	0
voronoi4_256	-3.706	6.06	0.001
a4_245, w4_256	-3.8	6	0
PM-64QAM	-3.09	6	0
a4_4096	-3.80	6.08	0.002

mappings have different tolerance to the NLI depending on the modulation format; we noted a strong impact of this mapping particularly on l4_13, c4_13, and l4_18 formats studied.

The reader interested in visualizing how 4D symbols map to each polarization is invited to see an exquisite demonstration in [37, Fig. 3] and [38, Fig. 2 (a)].

Two different mappings are shown in Fig. 3. The first one consists of mapping $c_{k,1}, c_{k,2}$ to the x polarization and the other two to the y. The second one maps $c_{k,1}, c_{k,4}$ to the x polarization and the other two to the y. The term Φ_1, given in Table II, for the second mapping is higher than for the first one, which explains why this mapping generates higher NLI. As can be seen in Fig. 3 (a), the NLI that disturbs l4_13 increases from around 37 dB for the first mapping to 37.55 dB for the second mapping, a difference of more than half a dB, surprisingly. There is also an increase of 0.20 dB in the NLI obtained via the second mapping compared to the first mapping in the case of c4_13, as indicated in Fig. 3 (b). This discrepancy for l4_18 is less, only about 0.10 dB, as shown in Fig. 3 (c). These results indicate that a good mapping of the constellation's coordinates to the polarization states might curb the impact of the NLI. Interestingly, the experienced NLI of the constellations presented in [37], [38] remains unchanged under different mappings.

V. CONCLUSION

A detailed derivation of a general analytical nonlinear model for 4D formats is given in this paper. The derived model has the ability to quantify the impact of Kerr nonlinearity on a 4D signal space, irrespective of symmetries. The interpolarization dependency had to be taken into account to derive this model. Numerical results show that the EGN model overestimates the NLI by around 1.4 dB in the case of c4_16 for a system with 80 WDM channels. This erroneous prediction is ascribed to polarization dependency, ignored in the EGN model. We also show that l4_16, c4_16 and SO-PMQPSK modulations have higher NLI than PM-QPSK; the SO-PMQPSK format experiences the highest NLI amongst 16-point constellations. Because the model can capture the nonlinear disturbance of an arbitrary 4D format, it it can uniquely be used to quantify the influence of a constellation's coordinates on the NLI. The model presented in this paper is valid for high dispersion regimes where the majority of the NLI stems from the XPM terms. Extending this model to transmissions over low-dispersion fiber is the subject of future research.

VI. APPENDIX

This appendix is devoted to evaluating $\sigma^2_{\text{XPM,x}}(\Omega)$ in (14) for a single pair of channels with fixed separation Ω. Thorough this section, the dependence on Ω is left out for notational convenience.

The variance of the perturbative term given in (8) can be written as

$$\begin{aligned}\sigma^2_{\text{XPM,x}} =& \frac{64}{81}\gamma^2 \sum_{h,k,l,h',k',l'} X_{h,k,l} X^*_{h',k',l'} \\ &\cdot \Big(4\mathbb{E}\{b_{h,\text{x}} b^*_{k,\text{x}} b^*_{h',\text{x}} b_{k',\text{x}}\}\mathbb{E}\{a_{l,\text{x}} a^*_{l',\text{x}}\} \\ &+ 2\mathbb{E}\{b_{h,\text{x}} b^*_{k,\text{x}} b^*_{h',\text{x}} b_{k',\text{y}}\}\mathbb{E}\{a_{l,\text{x}} a^*_{l',\text{y}}\} \\ &+ 2\mathbb{E}\{b_{h,\text{x}} b^*_{k,\text{x}} b^*_{h',\text{y}} b_{k',\text{y}}\}\mathbb{E}\{a_{l,\text{x}} a^*_{l',\text{x}}\} \\ &+ 2\mathbb{E}\{b_{h,\text{y}} b^*_{k,\text{y}} b^*_{h',\text{x}} b_{k',\text{x}}\}\mathbb{E}\{a_{l,\text{x}} a^*_{l',\text{x}}\} \\ &+ \mathbb{E}\{b_{h,\text{y}} b^*_{k,\text{y}} b^*_{h',\text{y}} b_{k',\text{y}}\}\mathbb{E}\{a_{l,\text{x}} a^*_{l',\text{x}}\} \\ &+ \mathbb{E}\{b_{h,\text{y}} b^*_{k,\text{y}} b^*_{h',\text{x}} b_{k',\text{y}}\}\mathbb{E}\{a_{l,\text{x}} a^*_{l',\text{y}}\} \\ &+ 2\mathbb{E}\{b_{h,\text{x}} b^*_{k,\text{y}} b^*_{h',\text{x}} b_{k',\text{x}}\}\mathbb{E}\{a_{l,\text{y}} a^*_{l',\text{x}}\} \\ &+ \mathbb{E}\{b_{h,\text{x}} b^*_{k,\text{y}} b^*_{h',\text{y}} b_{k',\text{y}}\}\mathbb{E}\{a_{l,\text{y}} a^*_{l',\text{x}}\} \\ &+ \mathbb{E}\{b_{h,\text{x}} b^*_{k,\text{y}} b^*_{h',\text{x}} b_{k',\text{y}}\}\mathbb{E}\{a_{l,\text{y}} a^*_{l',\text{y}}\} \Big). \end{aligned} \tag{21}$$

For the sake of brevity, we only give the procedure to calculate the second term of (21), and the same approach can be followed for the other terms. We focus on calculating this term because it is more general to compute than the first term. The second term is

$$\begin{aligned}\sigma^2_{\text{NLI,x,2nd}} =& \frac{64}{81}\gamma^2 \sum_{h,k,l,h',k',l'} X_{h,k,l} X^*_{h',k',l'} \\ &\cdot 2\mathbb{E}\{b_{h,\text{x}} b^*_{k,\text{x}} b^*_{h',\text{x}} b_{k',\text{y}}\}\mathbb{E}\{a_{l,\text{x}} a^*_{l',\text{y}}\}, \end{aligned} \tag{22}$$

where the second order moment $\mathbb{E}\{a_{l,\text{x}} a^*_{l',\text{y}}\} = \mathbb{E}\{a_{\text{x}} a^*_{\text{y}}\}\delta_{l,l'}$ (see [39, Appendix A]). To compute the fourth order moment, the following cases should be considered:

$$\begin{aligned}&\mathbb{E}\{b_{h,\text{x}} b^*_{k,\text{x}} b^*_{h',\text{x}} b_{k',\text{y}}\} \\ &= \begin{cases} \mathbb{E}\{|b_{\text{x}}|^2 b^*_{\text{x}} b_{\text{y}}\}, & h = k = h' = k' \\ \mathbb{E}\{|b_{\text{x}}|^2\}\mathbb{E}\{b^*_{\text{x}} b_{\text{y}}\}, & h = k \neq h' = k' \\ \mathbb{E}\{|b_{\text{x}}|^2\}\mathbb{E}\{b^*_{\text{x}} b_{\text{y}}\}, & h = h' \neq k = k' \\ \mathbb{E}\{b^{*2}_{\text{x}}\}\mathbb{E}\{b_{\text{x}} b_{\text{y}}\}, & h = k' \neq k = h'. \end{cases} \end{aligned} \tag{23}$$

Combining (6), (23), and (22) gives

$$\sigma^2_{\text{NLI,x,2nd}} = \frac{64}{81}\gamma^2 \int \frac{\mathrm{d}^3 w}{(2\pi)^3}\frac{\mathrm{d}^3 w'}{(2\pi)^3}$$
$$\cdot\, \rho(w_1,w_2,w_3)\rho^*(w_1',w_2',w_3')\Bigg(\Big(2\mathbb{E}\{|b_{\mathrm{x}}|^2 b_{\mathrm{x}}^* b_{\mathrm{y}}\}\mathbb{E}\{a_{\mathrm{x}}a_{\mathrm{y}}^*\}$$
$$\cdot \sum_h \mathrm{e}^{i(w_1-w_2-w_1'+w_2')hT} + 2\mathbb{E}\{|b_{\mathrm{x}}|^2\}\mathbb{E}\{b_{\mathrm{x}}^* b_{\mathrm{y}}\}\mathbb{E}\{a_{\mathrm{x}}a_{\mathrm{y}}^*\}$$
$$\cdot \sum_{h\neq h'} \mathrm{e}^{i(w_1-w_2)hT-(w_1'-w_2')h'T} + 2\mathbb{E}\{|b_{\mathrm{x}}|^2\}\mathbb{E}\{b_{\mathrm{x}}^* b_{\mathrm{y}}\}\mathbb{E}\{a_{\mathrm{x}}a_{\mathrm{y}}^*\}$$
$$\cdot \sum_{h\neq k} \mathrm{e}^{i(w_1-w_1')hT-(w_2-w_2')kT} + 2\mathbb{E}\{b_{\mathrm{x}}^{*2}\}\mathbb{E}\{b_{\mathrm{x}}b_{\mathrm{y}}\}\mathbb{E}\{a_{\mathrm{x}}a_{\mathrm{y}}^*\}$$
$$\cdot \sum_{h\neq k} \mathrm{e}^{i(w_1+w_2')hT-(w_2+w_1')kT}\Big)\sum_l \mathrm{e}^{i(w_3-w_3')lT}\Bigg). \tag{24}$$

Using [39, Eqs. (15) and (29)], we can write (24) as

$$\sigma^2_{\text{NLI,x,2nd}} = \frac{64}{81}\gamma^2 \int \frac{\mathrm{d}^3 w}{(2\pi)^3}\frac{\mathrm{d}^3 w'}{(2\pi)^3}\rho(w_1,w_2,w_3)\rho^*(w_1',w_2',w_3')$$
$$\cdot\Bigg(\Big(2\mathbb{E}\{|b_{\mathrm{x}}|^2 b_{\mathrm{x}}^* b_{\mathrm{y}}\}\mathbb{E}\{a_{\mathrm{x}}a_{\mathrm{y}}^*\}\frac{4\pi^2}{T^2}\delta(w_1-w_2-w_1'+w_2')$$
$$\cdot +2\mathbb{E}\{|b_{\mathrm{x}}|^2\}\mathbb{E}\{b_{\mathrm{x}}^* b_{\mathrm{y}}\}\mathbb{E}\{a_{\mathrm{x}}a_{\mathrm{y}}^*\}\frac{2\pi}{T}\Big(\frac{4\pi^2}{T^2}\delta(w_1-w_2)\delta(w_1'-w_2')$$
$$-\frac{2\pi}{T}\delta(w_1-w_2-w_1'+w_2')\Big)$$
$$\cdot +2\mathbb{E}\{|b_{\mathrm{x}}|^2\}\mathbb{E}\{b_{\mathrm{x}}^* b_{\mathrm{y}}\}\mathbb{E}\{a_{\mathrm{x}}a_{\mathrm{y}}^*\}\frac{2\pi}{T}\Big(\frac{4\pi^2}{T^2}\delta(w_1-w_1')\delta(w_2-w_2')$$
$$-\frac{2\pi}{T}\delta(w_1-w_2-w_1'+w_2')\Big)$$
$$+\,2\mathbb{E}\{b_{\mathrm{x}}^{*2}\}\mathbb{E}\{b_{\mathrm{x}}b_{\mathrm{y}}\}\mathbb{E}\{a_{\mathrm{x}}a_{\mathrm{y}}^*\}\frac{2\pi}{T}\Big(\frac{4\pi^2}{T^2}\delta(w_1+w_2')\delta(w_2+w_1')$$
$$-\frac{2\pi}{T}\delta(w_1-w_2-w_1'+w_2')\Big)\delta(w_3-w_3')\Bigg). \tag{25}$$

The term involving $\delta(w_1-w_2)\delta(w_1'-w_2')$ is a bias term resulting in a constant phase shift, and should be ignored [7, Sec. VIII, Eqs. (63)–(67)], [8, Sec. 3, Eq. (17)], [9, Appendix A], [40, Sec.IV-B and the text after (63)], [4, Appendix C]) and [20, Eq. (37)]. By removing this term from (25), we have

$$\sigma^2_{\text{NLI,x,2nd}} = \frac{64}{81}\Big[\Big(\mathbb{E}\{|b_{\mathrm{x}}|^2 b_{\mathrm{x}}^* b_{\mathrm{y}}\} - \mathbb{E}\{|b_{\mathrm{x}}|^2\}\mathbb{E}\{b_{\mathrm{x}}^* b_{\mathrm{y}}\}$$
$$-\mathbb{E}\{|b_{\mathrm{x}}|^2\}\mathbb{E}\{b_{\mathrm{x}}^* b_{\mathrm{y}}\} - \mathbb{E}\{b_{\mathrm{x}}^{*2}\}\mathbb{E}\{b_{\mathrm{x}}b_{\mathrm{y}}\}\Big)$$
$$\cdot\,\mathbb{E}\{a_{\mathrm{x}}a_{\mathrm{y}}^*\}2\chi_1 + \mathbb{E}\{|b_{\mathrm{x}}|^2\}\mathbb{E}\{b_{\mathrm{x}}^* b_{\mathrm{y}}\}\mathbb{E}\{a_{\mathrm{x}}a_{\mathrm{y}}^*\}2Z$$
$$+\,\mathbb{E}\{b_{\mathrm{x}}^{*2}\}\mathbb{E}\{b_{\mathrm{x}}b_{\mathrm{y}}\}\mathbb{E}\{a_{\mathrm{x}}a_{\mathrm{y}}^*\}2\chi_2\Big], \tag{26}$$

where χ_1, Z and χ_2 are expressed in Table I. The same approach can be employed for the other terms in (21). Using the fact that $\mathbb{E}\{|a_{\mathrm{x}}|^2\} = \mathbb{E}\{|b_{\mathrm{x}}|^2\} = P_{\mathrm{x}}$, (21) is expressed as (14).

REFERENCES

[1] A. Splett, C. Kurtzke, and K. Petermann, "Ultimate transmission capacity of amplified optical fiber communication systems taking into account fiber nonlinearities," in *Proc. European Conf. Optical Communication*, Montreux, Switzerland, Sep. 1993.

[2] K. Peddanarappagari and M. Brandt-Pearce, "Volterra series transfer function of single-mode fibers," *J. Lightw. Technol.*, vol. 15, no. 12, pp. 2232–2241, Dec. 1997.

[3] A. Carena, V. Curri, G. Bosco, P. Poggiolini, and F. Forghieri, "Modeling of the impact of nonlinear propagation effects in uncompensated optical coherent transmission links," *J. Lightw. Technol.*, vol. 30, no. 10, pp. 1524–1539, May 2012.

[4] P. Johannisson and M. Karlsson, "Perturbation analysis of nonlinear propagation in a strongly dispersive optical communication system," *J. Lightw. Technol.*, vol. 31, no. 8, pp. 1273–1282, Apr. 2013.

[5] L. Beygi, E. Agrell, P. Johannisson, M. Karlsson, and H. Wymeersch, "A discrete-time model for uncompensated single-channel fiber-optical links," *IEEE Trans. Commun.*, vol. 60, no. 11, pp. 3440–3450, Nov. 2012.

[6] S. Kumar and D. Yang, "Second-order theory for self-phase modulation and cross-phase modulation in optical fibers," *J. Lightw. Technol.*, vol. 23, no. 6, pp. 2073–2080, June 2005.

[7] A. Mecozzi and R. J. Essiambre, "Nonlinear Shannon limit in pseudolinear coherent systems," *J. Lightw. Technol.*, vol. 30, no. 12, pp. 2011–2024, June 2012.

[8] R. Dar, M. Feder, A. Mecozzi, and M. Shtaif, "Properties of nonlinear noise in long, dispersion-uncompensated fiber links," *Opt. Express*, vol. 21, no. 22, pp. 25 685–25 699, Nov. 2013.

[9] A. Carena, G. Bosco, V. Curri, Y. Jiang, P. Poggiolini, and F. Forghieri, "EGN model of non-linear fiber propagation," *Opt. Express*, vol. 22, no. 13, pp. 16 335–16 362, June 2014.

[10] I. Roberts, J. M. Kahn, J. Harley, and D. W. Boertjes, "Channel power optimization of WDM systems following Gaussian noise nonlinearity model in presence of stimulated Raman scattering," *J. Lightw. Technol.*, vol. 35, no. 23, pp. 5237–5249, Dec. 2017.

[11] D. Semrau, R. I. Killey, and P. Bayvel, "The Gaussian noise model in the presence of inter-channel stimulated Raman scattering," *J. Lightw. Technol.*, vol. 36, no. 14, July 2018.

[12] D. Semrau, R. I. Killey, and P. Bayvel, "A closed-form approximation of the Gaussian noise model in the presence of inter-channel stimulated Raman scattering," *J. Lightw. Technol.*, vol. 37, no. 9, pp. 1924–1936, May 2019.

[13] D. Semrau, E. Sillekens, R. I. Killey, and P. Bayvel, "A modulation format correction formula for the Gaussian noise model in the presence of inter-channel stimulated Raman scattering," *J. Lightw. Technol.*, vol. 37, no. 19, pp. 5122–5131, Oct. 2019.

[14] ——, "Corrections to 'A modulation format correction formula for the Gaussian noise model in the presence of inter-channel stimulated Raman scattering'," *J. Lightw. Technol.*, vol. 38, no. 6, pp. 1604–1604, Mar. 2020.

[15] P. Serena, C. Lasagni, S. Musetti, and A. Bononi, "On numerical simulations of ultra-wideband long-haul optical communication systems," *J. Lightw. Technol.*, vol. 38, no. 5, pp. 1019–1031, Sep. 2019.

[16] H. Rabbani, G. Liga, V. Oliari, L. Beygi, E. Agrell, M. Karlsson, and A. Alvarado, "A general analytical model of nonlinear fiber propagation in the presence of Kerr nonlinearity and stimulated Raman scattering," *arXiv preprint arXiv:1909.08714v2*, June 2020.

[17] G. Rademacher and K. Petermann, "Nonlinear Gaussian noise model for multimode fibers with space-division multiplexing," *J. Lightw. Technol.*, vol. 34, no. 9, pp. 2280–2287, May 2016.

[18] C. Antonelli, M. Shtaif, and A. Mecozzi, "Modeling of nonlinear propagation in space-division multiplexed fiber-optic transmission," *J. Lightw. Technol.*, vol. 34, no. 1, pp. 36–54, Jan. 2016.

[19] C. Antonelli, O. Golani, M. Shtaif, and A. Mecozzi, "Nonlinear interference noise in space-division multiplexed transmission through optical fibers," *Opt. Express*, vol. 25, no. 12, pp. 13 055–13 078, June 2017.

[20] H. Rabbani, M. Ayaz, L. Beygi, G. Liga, A. Alvarado, E. Agrell, and M. Karlsson, "Analytical modeling of nonlinear fiber propagation for four dimensional symmetric constellations," *J. Lightw. Technol.*, vol. 39, no. 9, pp. 2704–2713, May 2021.

[21] H. Rabbani, H. Hossienianfar, and M. Brandt-Pearce, "An enhanced analytical model of nonlinear fiber effects for four-dimensional symmetric modulation formats," *J. Lightw. Technol.*, pp. 1–8, June 2022.

[22] G. Liga, A. Barreiro, H. Rabbani, and A. Alvarado, "Extending fibre nonlinear interference power modelling to account for general dual-polarisation 4D modulation formats," *Entropy*, vol. 22, no. 11, p. 1324, Nov. 2020.

[23] E. Ip, "Nonlinear compensation using backpropagation for polarization-multiplexed transmission," *J. Lightw. Technol.*, vol. 28, no. 6, pp. 939–951, Mar. 2010.

[24] H. Rabbani, H. Rabbani, L. Beygi, and E. Agrell, "Improving the achievable rates of optical coherent transmission with back-propagation," *IEEE Photon. Technol. Lett.*, July 2018.
[25] P. Poggiolini, A. Nespola, Y. Jiang, G. Bosco, A. Carena, L. Bertignono, S. M. Bilal, S. Abrate, and F. Forghieri, "Analytical and experimental results on system maximum reach increase through symbol rate optimization," *J. Lightw. Technol.*, vol. 34, no. 8, pp. 1872–1885, Apr. 2016.
[26] M. Karlsson and E. Agrell, "Spectrally efficient four-dimensional modulation," *in Proc. Optic. Fiber Commun. Conf.*, Mar. 2012, OTu2C.1.
[27] P. Wai and C. Menyak, "Polarization mode dispersion, decorrelation, and diffusion in optical fibers with randomly varying birefringence," *J. Lightw. Technol.*, vol. 14, no. 2, pp. 148–157, Feb. 1996.
[28] R. Dar, M. Feder, A. Mecozzi, and M. Shtaif, "Inter-channel nonlinear interference noise in WDM systems: Modeling and mitigation," *J. Lightw. Technol.*, vol. 33, no. 5, pp. 1044–1053, Mar. 2015.
[29] M. Sjodin, E. Agrell, and M. Karlsson, "Subset-optimized polarization-multiplexed PSK for fiber-optic communications," *IEEE Commun. Lett.*, vol. 17, no. 5, pp. 838–840, May 2013.
[30] E. Agrell, "Database of sphere packings," 2016. [Online]. Available: http://codes.se/packings/.
[31] M. Karlsson and E. Agrell, "Four-dimensional optimized constellations for coherent optical transmission systems," in *Proc. European Conf. Optical Communication*, Turin, Italy, Sep. 2010.
[32] A. Alvarado and E. Agrell, "Four-dimensional coded modulation with bit-wise decoders for future optical communications," *J. Lightw. Technol.*, vol. 33, no. 10, pp. 1993–2003, May 2015.
[33] J. H. Conway and N. J. A. Sloane, *Sphere Packings, Lattices and Groups*, 3rd ed. Springer-Verlag, 1998.
[34] G. D. Forney, Jr., "Multidimensional constellations. II. Voronoi constellations," *IEEE J. Select. Areas Commun.*, vol. 7, no. 6, pp. 941–958, Aug. 1989.
[35] T. A. Eriksson, S. Alreesh, C. Schmidt-Langhorst, F. Frey, P. W. Berenguer, C. Schubert, J. K. Fischer, P. A. Andrekson, M. Karlsson, and E. Agrell, "Experimental investigation of a four-dimensional 256-ary lattice-based modulation format," in *Proc. Optical Fiber Communication Conf.*, Los Angeles, CA, USA, Mar. 2015.
[36] G. Welti and J. Lee, "Digital transmission with coherent four-dimensional modulation," *IEEE Trans. Inform. Theory*, Jul. 1974.
[37] B. Chen, C. Okonkwo, H. Hafermann, and A. Alvarado, "Polarization-ring-switching for nonlinearity-tolerant geometrically shaped four-dimensional formats maximizing generalized mutual information," *J. Lightw. Technol.*, vol. 37, no. 14, pp. 3579–3591, July 2019.
[38] B. Chen, A. Alvarado, S. van der Heide, M. van den Hout, H. Hafermann, and C. Okonkwo, "Analysis and experimental demonstration of orthant-symmetric four-dimensional 7 bit/4d-sym modulation for optical fiber communication," *J. Lightw. Technol.*, vol. 39, no. 9, pp. 2737–2753, May 2021.
[39] O. Golani, R. Dar, M. Feder, A. Mecozzi, and M. Shtaif, "Modeling the bit-error-rate performance of nonlinear fiber-optic systems," *J. Lightw. Technol.*, vol. 34, no. 15, pp. 3482–3489, Aug. 2016.
[40] P. Poggiolini, G. Bosco, A. Carena, V. Curri, Y. Jiang, and F. Forghieri, "A detailed analytical derivation of the GN model of non-linear interference in coherent optical transmission systems," *arXiv preprint arXiv:1209.0394*, June 2014.